agreement with recent theory[20] make the former possibility attractive, we cannot rule out the latter without comparison to a more complete calculation of charge noise in QDs.

We have also examined non-equilibrium charge fluctuations in a second sample (S2). We modified our design by removing the 2DEG immediately to the left of the dot with a wet etch (inset, Fig. 4a). Doing so does not prevent formation of a QD (Fig. 4b), and allows us to observe switching due to tunnelling between the dot and its source and drain. Both a time-domain analysis and d.c. current measurement (Fig. 4a) show a wide Coulomb-blockade region near zero bias. As the bias increases, the counts N_c detected by the RF-SET rise first, followed later by a detectable current I. This is in agreement with the single level model discussed above, which gives $I \approx e\Gamma_S\Gamma_D f(E_S)/(\Gamma_S + \Gamma_D)$ when, for example, the source is close to resonance with an unoccupied dot level (Fig. 4c). Here Γ_S and Γ_D are the couplings between the dot and its source and drain and $E_S = 2E_{C_{QD}}\left(\frac{1}{2} - \frac{Q_{QD}}{e}\right) + \frac{1}{2}eV_{SD}$. The corresponding expression for N_c scaled to units of current is $N_c e/2\Delta t = e\Gamma_S f(E_S)\{\Gamma_D + [1 - f(E_S)]\Gamma_S\}/(\Gamma_S + \Gamma_D)$; the factor of two on the left accounts for the two transitions an electron makes entering and leaving the dot. The current senses only electrons that traverse the dot. In contrast, N_c includes electrons that enter and leave the dot through the same junction (second term in curly brackets), that is, the RF-SET also detects thermal charge fluctuations at the source junction (Fig. 4c). If $\Gamma_S \approx \Gamma_D$, the two terms make roughly equal contributions to N_c just below threshold, and $N_c e/2\Delta t > I$ as measured.

Received 16 January; accepted 7 April 2003; doi:10.1038/nature01642.

1. Ben-Jacob, E. & Gefen, Y. New quantum oscillations in current driven small junctions. *Phys. Lett. A* **108,** 289–292 (1985).
2. Delsing, P., Likharev, K. K., Kuzmin, L. S. & Claeson, T. Time-correlated single-electron tunneling in one-dimensional arrays of ultrasmall tunnel junctions. *Phys. Rev. Lett.* **63,** 1861–1864 (1989).
3. Dresselhaus, P. D., Ji, L., Han, S., Lukens, J. E. & Likharev, K. K. Measurement of single electron lifetimes in a multijunction trap. *Phys. Rev. Lett.* **72,** 3226–3229 (1994).
4. Berman, D., Zhitenev, N. B., Ashoori, R. C. & Shayegan, M. Observation of quantum fluctuations of charge on a quantum dot. *Phys. Rev. Lett.* **82,** 161–164 (1999).
5. Blanter, Y. M. & Büttiker, M. Shot noise in mesoscopic conductors. *Phys. Rep.* **336,** 1–166 (2000).
6. Levitov, L. S. & Lesovik, G. B. Charge-transport statistics in quantum conductors. *JETP Lett.* **55,** 555–559 (1992).
7. Levitov, L. S., Lee, H. & Lesovik, G. B. Electron counting statistics and coherent states of electric current. *J. Math. Phys.* **37,** 4845–4866 (1996).
8. Shnirman, A. & Schön, G. Quantum measurements performed with a single-electron transistor. *Phys. Rev. B* **57,** 15400–15407 (1998).
9. Loss, D. & DiVincenzo, D. P. Quantum computation with quantum dots. *Phys. Rev. A* **57,** 120–126 (1998).
10. Schoelkopf, R. J., Wahlgren, P., Kozhevnikov, A. A., Delsing, P. & Prober, D. E. The radio-frequency single-electron transistor (RF-SET): A fast and ultrasensitive electrometer. *Science* **280,** 1238–1242 (1998).
11. Aassime, A., Johansson, G., Wendin, G., Schoelkopf, R. J. & Delsing, P. Radio-frequency single-electron transistor as readout device for qubits: Charge sensitivity and backaction. *Phys. Rev. Lett.* **86,** 3376–3379 (2001).
12. Likharev, K. K. Single-electron transistors: Electrostatic analogs of the DC SQUIDS. *IEEE Trans. Magn.* **23,** 1142–1145 (1987).
13. Fulton, T. A. & Dolan, G. J. Observation of single-electron charging effects in small tunnel junctions. *Phys. Rev. Lett.* **59,** 109–112 (1987).
14. Kirton, M. J. & Uren, M. J. Noise in solid-state microstructures: A new perspective on individual defects, interface states, and low-frequency (1/*f*) noise. *Adv. Phys.* **38,** 367–468 (1989).
15. Fujisawa, T. & Hirayama, Y. Charge noise analysis of an AlGaAs/GaAs quantum dot using transmission-type radio-frequency single-electron transistor technique. *Appl. Phys. Lett.* **77,** 543–545 (2000).
16. Basseville, M. & Nikiforov, I. V. *Detection of Abrupt Changes* (Prentice Hall, Englewood Cliffs, 1993).
17. Lu, W., Rimberg, A. J., Maranowski, K. D. & Gossard, A. C. A single-electron transistor strongly coupled to an electrostatically defined quantum dot. *Appl. Phys. Lett.* **77,** 2746–2748 (2000).
18. Folk, J. A., Marcus, C. M. & Harris, J. S. Decoherence in nearly isolated quantum dots. *Phys. Rev. Lett.* **87,** 206802 (2001).
19. Eisenberg, E., Held, K. & Altshuler, B. L. Dephasing times in closed quantum dots. *Phys. Rev. Lett.* **88,** 136801 (2002).
20. Altshuler, B. L., Gefen, Y., Kamenev, A. & Levitov, L. S. Quasiparticle lifetime in a finite system: A nonperturbative approach. *Phys. Rev. Lett.* **78,** 2803–2806 (1997).
21. Beenakker, C. W. J. Theory of Coulomb-blockade oscillations in the conductance of a quantum dot. *Phys. Rev. B* **44,** 1646–1656 (1991).

Acknowledgements We thank W. L. Wilson, M. Thalakulam, J. Sarkar, R. J. Schoelkopf, D. H. Johnson, D. Natelson, R. M. Westervelt, D. Driscoll and A. C. Gossard for discussions and experimental assistance. This work was supported by the National Science Foundation, the Army Research Office, and the Robert A. Welch Foundation.

Competing interests statement The authors declare that they have no competing financial interests.

Correspondence and requests for materials should be addressed to A.R. (rimberg@rice.edu).

Spin entropy as the likely source of enhanced thermopower in $Na_xCo_2O_4$

Yayu Wang*, Nyrissa S. Rogado†, R. J. Cava†‡ & N. P. Ong*‡

** Department of Physics, † Department of Chemistry, ‡ Princeton Materials Institute, Princeton University, Princeton, New Jersey 08544, USA*

In an electric field, the flow of electrons in a solid produces an entropy current in addition to the familiar charge current. This is the Peltier effect, and it underlies all thermoelectric refrigerators. The increased interest in thermoelectric cooling applications has led to a search for more efficient Peltier materials and to renewed theoretical investigation into how electron–electron interaction may enhance the thermopower of materials such as the transition-metal oxides[1–4]. An important factor in this enhancement is the electronic spin entropy, which is predicted[4–6] to dominate the entropy current. However, the crucial evidence for the spin-entropy term, namely its complete suppression in a longitudinal magnetic field, has not been reported until now. Here we report evidence for such suppression in the layered oxide $Na_xCo_2O_4$, from thermopower and magnetization measurements in both longitudinal and transverse magnetic fields. The strong dependence of thermopower on magnetic field provides a rare, unambiguous example of how strong electron–electron interaction effects can qualitatively alter electronic behaviour in a solid. We discuss the implications of our finding—that spin-entropy dominates the enhancement of thermopower in transition-metal oxides—for the search for better Peltier materials.

In a thermopower experiment, a temperature gradient $-\nabla T$ drives the diffusion of charge carriers to the cooler end of the sample. The charge accumulation leads to a net electric field E which determines the thermopower (or Seebeck coefficient) $Q = E/|\nabla T|$ (ref. 7). In conventional metals, the flow of electrons induced by $-\nabla T$ is nearly cancelled by a parallel flow of holes, so that Q is strongly reduced by the factor T/T_F from the 'natural value' $k_B/e \approx 86\,\mu V\,K^{-1}$, where k_B is Boltzmann's constant, e the electron charge and T_F the Fermi temperature[7]. Moreover, as the currents are indifferent to the spins, a longitudinal magnetic field $\mathbf{H} \| -\nabla T$ has almost no effect on Q. In materials with strong electron–electron interaction, however, the spin degrees are predicted to produce a large contribution of the Heikes form[2,4,6]:

$$Q = \mu/eT = -\sigma/e \quad (1)$$

where μ is the chemical potential, and σ (the entropy per electron)

equals $k_B \ln(g_s g_c)$ with g_s and g_c the spin and configuration degeneracies, respectively. From equation (1), the enhancement to Q from spin entropy is of the order k_B/e, but it is suppressed to zero if the spin degeneracy is lifted in a magnetic field ($g_s \rightarrow 1$).

Q in $Na_xCo_2O_4$ (at 300 K) is about ten times larger than in typical metals[8]. The role of spin fluctuations, as in heavy-fermion systems, has been suggested[8]. Despite Hall effect[8], heat capacity[9] and nuclear spin-resonance[10] experiments, however, the enhancement in Q remains puzzling. Experiments have not ruled out either strong-interaction theories involving spin configurations[11], or conventional interpretations based on small Fermi surfaces[12]. By investigating the thermopower and magnetization in both longitudinal and transverse H, we show that $Na_xCo_2O_4$ is in fact a strong-correlation system in which the spin entropy term accounts for almost all of Q at 2 K and a dominant fraction at 300 K.

In $Na_xCo_2O_4$, the Co ions occupy the sites of a two-dimensional (2D) triangular lattice. Chemical arguments and band-structure calculations[12] show that the O 2p states lie far below the Co 3d states and the chemical potential falls within the band formed from t_{2g} states in Co. Hence the electrons donated by Na ions are distributed among the Co ions, a fraction (δ) of which are in the Co^{4+} state, while the rest ($1 - \delta$) are Co^{3+}. From $x = 1.36$ (determined by inductively coupled plasma spectrometer (ICP) chemical analysis of our crystals), we find $\delta = 0.32$. The variation of the susceptibilities χ_{ab} and χ_c versus temperature T (upper inset in Fig. 1) fitted accurately to the Curie–Weiss form $1/(T + \theta)$, implying the existence of large local moments that are antiferromagnetically coupled. The plot of $1/\chi_{ab}$ gives $\theta = 55 \pm 5$ K and a moment around 0.87 μ_B averaged over all Co ions (μ_B is the Bohr magneton). This experimentally constrains the Co^{4+} ions to be in the low-spin state, with spin $S = 1/2$ and moment $\sqrt{3}\,\mu_B$, while the Co^{3+} ions are in their low-spin $S = 0$ state (Fig. 1, lower inset), in agreement with ref. 10.

The in-plane resistivity ρ displays a T-linear variation below 100 K that is suggestive of strong-correlation behaviour (dashed line in Fig. 1). As noted in ref. 8, Q (circles in Fig. 1) increases with T to values much larger than in conventional metals. However, it is the effect of a magnetic field on Q that is the most informative. The pronounced effect of an in-plane field **H** on Q is shown in Fig. 2($\mathbf{H} \| -\nabla T$). Stringent precautions against spurious contributions to Q were adopted (see Supplementary Information). Even at moderately high T (30 K), Q decreases significantly in a 14-T field. Lowering the temperature makes the field-suppression of Q more pronounced, until at 4 K, Q changes sign and saturates near 12 T to a 'floor' value equal to $-0.25\,\mu V\,K^{-1}$. With further decrease in T, the floor value itself monotonically decreases to zero. The trace at 2.5 K shows that Q decreases monotonically to zero in a field of 8 T, and remains at zero over an extended field range.

The strong effect of field on Q is also observed with $\mathbf{H} \| \mathbf{c}$ (normal to plane), except that, above 6 K, we observe an additional term that produces an increase in Q in weak fields. At 4.2 K, Q displays the same field profile as above, but with a proportionately weaker decrease (Fig. 3). As the sample is warmed to 10 K and higher, the relative change in Q is initially positive in low fields. At higher fields,

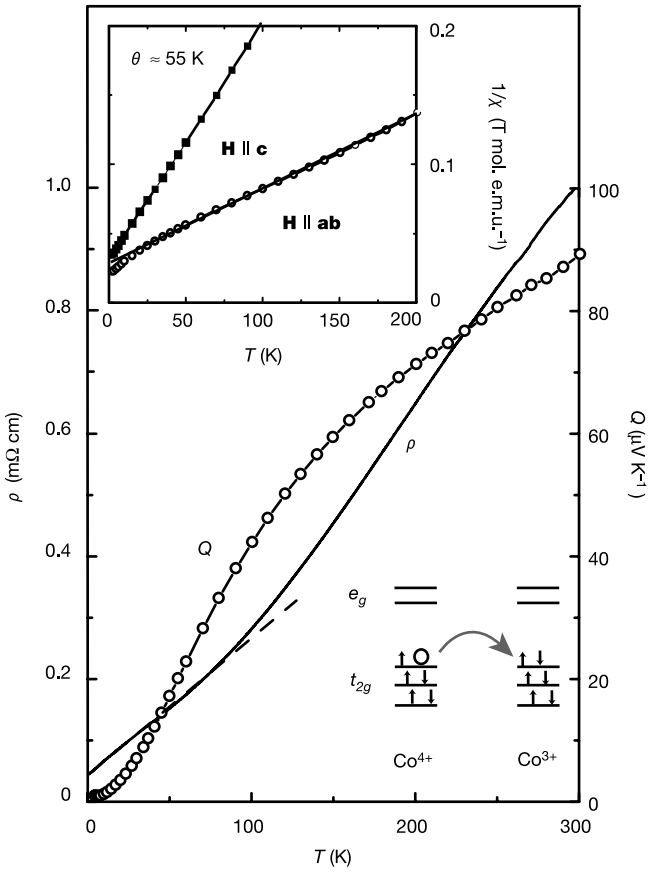

Figure 1 The temperature (T) dependence of magnetic and transport properties of single-crystal $Na_xCo_2O_4$ and electronic states in the Co ions. The in-plane thermopower Q (circles) and resistivity ρ (solid curve) are plotted versus T. The T-linear dependence of ρ below 100 K is indicated by the dashed line. The upper inset shows the T dependence of the inverse susceptibilities χ_{ab} and χ_c measured in a 5-T field applied in-plane and along the c axis, respectively. The lower inset is a sketch of the low-spin t_{2g} states in the Co^{4+} and Co^{3+} ions. The hopping of a hole (arrow) is accompanied by the transfer of a spin-1/2 excitation.

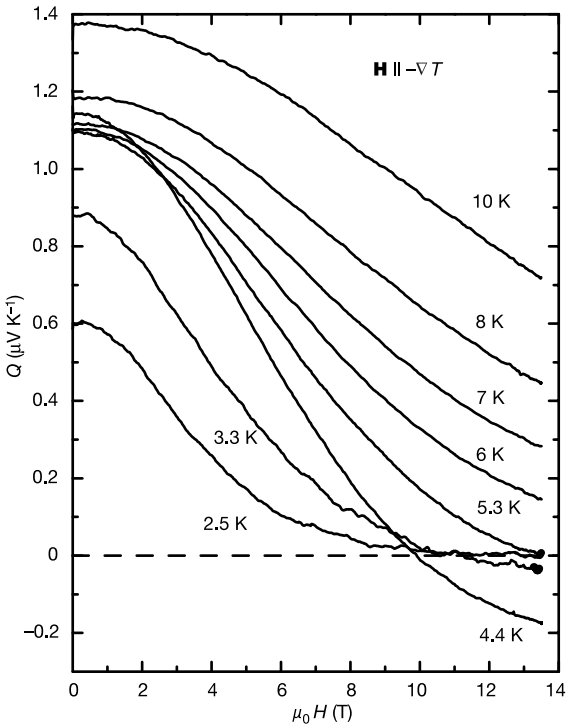

Figure 2 The in-plane thermopower Q versus an in-plane $\mathbf{H} \| (-\nabla T)$ at selected T. At 4.4 K, Q tends asymptotically at high fields to a negative floor value ($-0.25\,\mu V\,K^{-1}$). At the lowest T (2.5 K), Q approaches a value unresolved from zero when H exceeds 8 T. The applied temperature difference δT is less than 0.3 K below 4 K, and about 0.5 K above 4 K. By using phosphor bronze as the voltage leads, we have eliminated background contributions to Q (Supplementary Information).

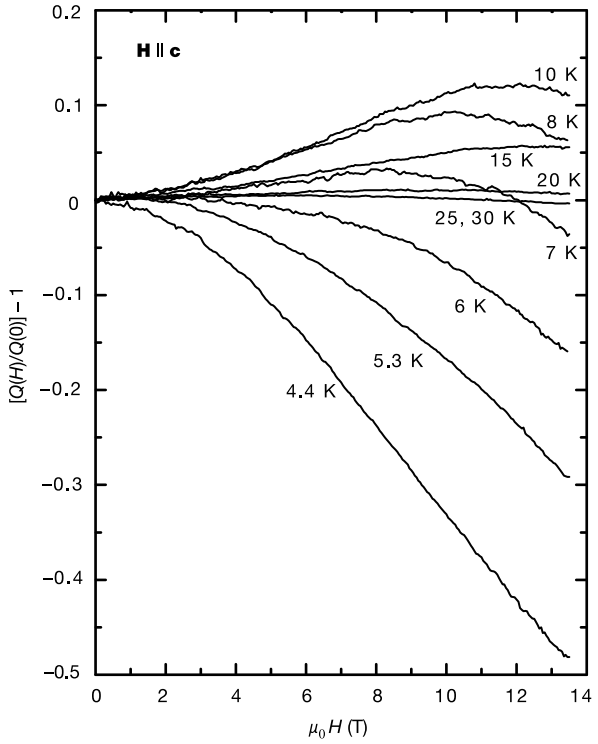

Figure 3 The relative change in Q versus a transverse field **H||c** in $Na_xCo_2O_4$. At 6 K and lower, Q decreases monotonically with H, but at higher temperatures, Q initially increases in weak field before decreasing at larger H.

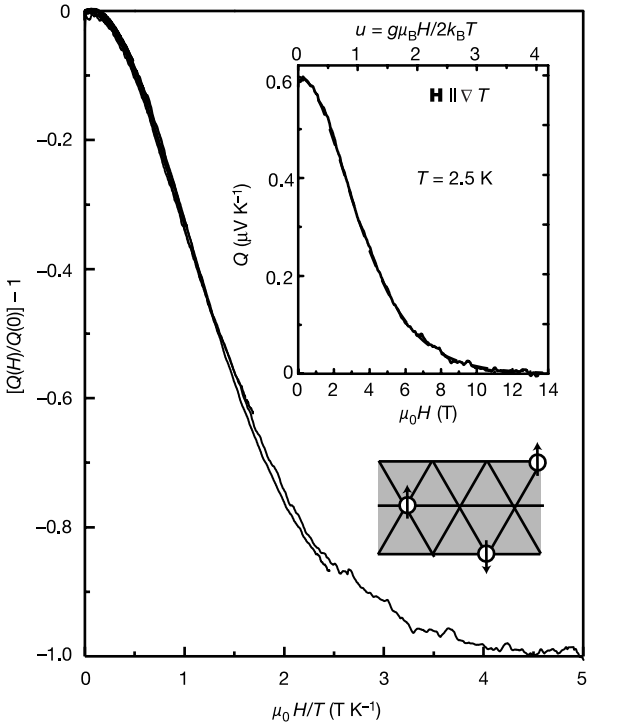

Figure 4 The suppression of the thermopower by an in-plane magnetic field in $Na_xCo_2O_4$. The normalized Q is plotted versus $\mu_0 H/T$. Curves measured at various T values (2.5, 6, 8, 10, 12.5, 15, 20 and 25 K) collapse to a universal curve. The lower inset shows the spin-1/2 excitations in an inert background of Co^{3+} ions. The upper inset compares the data curve at 2.5 K (solid curve) with the expression in equation (2) (dashed curve).

the negative trend again becomes apparent. The overall pattern in transverse field is consistent with a positive contribution superposed on the term intrinsic to the spin degrees uncovered in the longitudinal field.

The evidence that the H dependence of Q arises from the spin degrees of freedom derives from both the transport and susceptibility experiments. Because an in-plane field couples to the spin degrees only, but not to the orbital degrees, the strong H dependence of Q in Fig. 3 must arise from the effect of field on the spins. In the geometry with **H||c**, we reason that the non-monotonic field dependence of Q also arises entirely from the effect of H on the spin degrees, as the carrier mean-free path $l \approx 100$ Å estimated from ρ is far too short to produce any orbital effect in a field of 14 T. Comparing curves at 4 K in Figs 2 and 3, we infer that a similar decrease in Q requires a c-axis field that is 1.4 times larger than the in-plane field. The close agreement between this ratio and the ratio of the bulk susceptibilities χ_{ab}/χ_c at 4 K strongly suggests that the field anisotropies in the magnetization and thermopower experiments have the same origin. The field suppression of Q is larger with the field in-plane compared with the field along the c axis because it is easier to align the spins with an in-plane field.

In conventional metals, a longitudinal field merely changes the relative populations of the spin-up (+) and spin-down (−) electrons without significantly altering the entropy current in each spin population[7]. The complete suppression displayed in Fig. 2 is incompatible with a conventional band picture.

We next discuss how the field suppression may be understood within a strong-correlation scenario. As shown in the lower inset of Fig. 4, in the 2D triangular lattice of the Co ions, a fraction $\delta = 1/3$ are in the Co^{4+} state in which $S = 1/2$, while the rest are in the Co^{3+} state with $S = 0$ (the higher-lying e_g orbitals are unoccupied). The elementary charge-transport process is the hopping of a hole from Co^{4+} to Co^{3+} (Fig. 1, lower inset). A large on-site repulsion excludes double occupancy of a site by the holes. Because this process converts the Co^{4+} ($S = 1/2$) to a Co^{3+} ($S = 0$) and vice versa, we also transfer a spin-1/2 along with the hole, which implies a transfer of spin entropy $\sigma = k_B \ln 2$ in zero field. The excitations are holes carrying charge $+1e$ and spin-1/2 moving in a sea of Co^{3+} sites, which are magnetically and electrically inert. An E field leads to the heat current $J_Q = nvk_BT\ln(2)$ as well as the charge current $J = nev$ (with n the hole concentration and v the average velocity). As the ratio J_Q/J (called the Peltier coefficient Π)[7] equals the product QT, we obtain the spin-entropy part of Q given in equation (1). Moreover, because the spin-entropy current is in the direction of the charge current, this contribution to Q is positive (hole-like) as observed.

As T decreases below $\theta \approx 50$ K (the antiferromagnetic exchange energy $J_{AF} \approx \theta$), the spin entropy must decrease rapidly with incipient magnetic ordering to vanish at $T = 0$. When $T \ll \theta$, the majority of the spins become antiferromagnetically correlated with their neighbours, leaving only a small fraction T/θ to behave as free spins. In an E field, this residual population of free spins carries the spin entropy, although all the holes remain itinerant. This implies that the ratio J_Q/J decreases steeply below θ, consistent with the observed behaviour of Q in Fig. 1.

In a magnetic field, the residual spin entropy $\sigma(H,T)$ is further decreased, eventually reaching zero when H is strong enough completely to lift the twofold degeneracy. Modelling the residual free spins as non-interacting spins with the Landé g-factor g, we calculate the field dependence of the entropy as:

$$\sigma(H,T)/\sigma(0,T) = \{\ln[2\cosh(u)] - u\tanh(u)\}/\ln(2) \qquad (2)$$

where $u = g\mu_B H/2k_B T$. This dependence should apply to the component of Q derived from the spin entropy.

As shown in Fig. 4, the curves of Q in Fig. 2 between 2.5 and 25 K can be collapsed onto a universal curve when plotted against the ratio H/T. Using the curve at 2.5 K (which extends to the largest u), we find that equation (2) provides a remarkably close fit if the Landé g-factor is 2.2 ± 0.1 (upper inset in Fig. 4). We view the close fit as confirming evidence that the entropy current observed in the thermopower indeed derives entirely from the spin-1/2 excitations, and the complete suppression of Q reflects the removal of the spin degeneracy by the applied field.

We note that, at each T, the observed Q is composed of several distinct contributions. Application of a strong longitudinal H completely suppresses only the spin-entropy term, leaving the remaining terms unaffected (the configuration entropy $k_B \ln g_c$, for instance) which are revealed as the floor value at high fields. In Fig. 2, these terms amount to $-0.25\,\mu V\,K^{-1}$ at 4.4 K and rapidly vanish at lower T. We emphasize that the spin entropy contribution to Q is not restricted to low T. Measurements at high fields (30 T) show that Q is suppressed by about 20% at 30 K. Assuming that, when $T \gg \theta$, the spin contribution asymptotes to $(k_B/e)\ln(2) \approx 60\,\mu V\,K^{-1}$, we find that it constitutes about two-thirds of the total thermopower at 300 K, thus accounting for most of the enhanced thermopower.

The spin-entropy enhancement may be widespread in the transition-metal oxides. A key ingredient inferred from our measurements is the motion of charge tied to local moments of spin-1/2 in a background of Co^{3+} ions that are magnetically inert (diamagnetic). Of the large class of cobalt oxides, the Co ions are nearly always in their low-spin state. In the Co oxides that can be made conducting, therefore, the thermopower is likely to be dominated by spin-entropy terms, suggesting that this is a promising class of materials to search for improved Peltier materials.

Received 28 January; accepted 28 March 2003; doi:10.1038/nature01639.

1. Mahan, G., Sales, B. & Sharp, J. Thermoelectric materials: New approaches to an old problem. *Phys. Today* **50**(3), 42–47 (1997).
2. Beni, G. Thermoelectric power of the narrow-band Hubbard chain at arbitrary electron density: Atomic limit. *Phys. Rev. B* **10,** 2186–2189 (1974).
3. Palsson, G. & Kotliar, G. Thermoelectric power near the density-driven Mott transition. *Phys. Rev. Lett.* **80,** 4775–4778 (1998).
4. Chaikin, P. M. & Beni, G. Thermopower in the correlated hopping regime. *Phys. Rev. B* **13,** 647–651 (1976).
5. Kwak, J. F. & Beni, G. Thermoelectric power of a Hubbard chain with arbitrary electron density: Strong-coupling limit. *Phys. Rev. B* **13,** 652–657 (1976).
6. Kwak, J. F., Beni, G. & Chaikin, P. M. Thermoelectric power in Hubbard-model systems with different densities: *N*-methylphenazimium-tetracyanoquinodimethane (NMP-TCNQ), and quinolinium ditetracyanoquinodimethane. *Phys. Rev. B* **13,** 641–646 (1976).
7. Ziman, J. M. *Principles of The Theory of Solids* 235 (Cambridge Univ. Press, London, 1972).
8. Terasaki, I., Sasago, Y. & Uchinokura, K. Large thermoelectric power in $NaCo_2O_4$ single crystals. *Phys. Rev. B* **56,** R12685–R12687 (1997).
9. Ando, Y., Miyamoto, N., Segawa, K., Kawata, T. & Terasaki, I. Specific-heat evidence for strong electron correlations in the thermoelectric material (Na,Ca) Co_2O_4. *Phys. Rev. B* **60,** 10580–10583 (1999).
10. Ray, R., Ghoshray, A., Ghoshray, K. & Nakamura, S. ^{59}Co NMR studies of metallic $NaCo_2O_4$. *Phys. Rev. B* **59,** 9454–9461 (1999).
11. Koshibae, W., Tsutsui, K. & Maekawa, S. Thermopower in cobalt oxides. *Phys. Rev. B* **62,** 6869–6872 (2000).
12. Singh, D. J. Electronic structure of $NaCo_2O_4$. *Phys. Rev. B* **61,** 13397–13402 (2000).

Supplementary Information accompanies the paper on **www.nature.com/nature**.

Acknowledgements We thank S. Hannahs for technical assistance. We acknowledge support from the US National Science Foundation (NSF). Some of the measurements were performed at the US National High Magnetic Field Laboratory, which is supported by the NSF and the state of Florida.

Competing interests statement The authors declare that they have no competing financial interests.

Correspondence and requests for materials should be addressed to N.P.O. (npo@princeton.edu).

^{146}Sm–^{142}Nd evidence from Isua metamorphosed sediments for early differentiation of the Earth's mantle

Guillaume Caro*, Bernard Bourdon*, Jean-Louis Birck* & Stephen Moorbath†

* *Laboratoire de Géochimie et Cosmochimie (UMR 7579 CNRS), Institut de Physique du Globe de Paris, Université Denis Diderot, 4 place Jussieu, 75252 Paris Cedex 05, France*

† *Department of Earth Sciences, Oxford University, Parks Road, Oxford OX1 3PR, UK*

Application of the ^{147}Sm–^{143}Nd chronometer (half-life of 106 Gyr) suggests that large-scale differentiation of the Earth's mantle may have occurred during the first few hundred million years of its history[1]. However, the signature of mantle depletion found in early Archaean rocks is often obscured by uncertainties resulting from open-system behaviour of the rocks during later high-grade metamorphic events[2]. Hence, although strong hints exist regarding the presence of differentiated silicate reservoirs before 4.0 Gyr ago, both the nature and age of early mantle differentiation processes remain largely speculative[3–5]. Here we apply short-lived ^{146}Sm–^{142}Nd chronometry (half-life of 103 Myr) to early Archaean rocks using ultraprecise measurement of Nd isotope ratios. The analysed samples are well-preserved metamorphosed sedimentary rocks from the 3.7–3.8-Gyr Isua greenstone belt of West Greenland. All display well-resolved ^{142}Nd anomalies averaging 15 ± 4 p.p.m. (2σ). Using the initial ε^{143}Nd value from ref. 6 coupled ^{146}Sm–^{147}Sm chronometry constrains the mean age of mantle differentiation to 4,460 ± 115 Myr. This early Sm/Nd fractionation probably reflects differentiation of the Earth's mantle during the final stage of terrestrial accretion.

Short-lived radioactive nuclides are ideal tools to constrain early differentiation of the main terrestrial reservoirs. The ^{129}I–^{129}Xe (half-life 16 Myr) chronometer constrains mantle degassing and formation of the atmosphere to the first 100 Myr of Earth history[7], and ^{182}Hf–^{182}W systematics (half-life 9 Myr) provide clear evidence that core segregation occurred during the first 30 Myr of terrestrial accretion[8–10]. Similarly, the short-lived ^{146}Sm–^{142}Nd chronometer has long been viewed as a promising tracer for exploring the early history of the Earth's mantle. The presence of live ^{146}Sm in the early Solar System was first demonstrated by Lugmair *et al.*[11], and its initial abundance subsequently defined as ^{146}Sm/^{144}Sm = 0.008 ± 1 at 4.566 Gyr ago[12]. Because of its low initial abundance, ^{146}Sm is effectively extinct after 4–5 half-lives, so that ^{142}Nd/^{144}Nd anomalies can be related solely to differentiation of silicate reservoirs during the first few hundred million years of Earth history. Additionally, the ^{142}Nd signature of early Archaean rocks is insensitive to metamorphic disturbances, so that ^{146}Sm–^{142}Nd chronometry can be reliably applied to a wide range of crustal rocks.

However, in view of the low initial abundance of ^{146}Sm, ^{142}Nd anomalies are expected to be extremely small (less than 30–40 p.p.m.), and their detection requires ultraprecise Nd isotope measurements. Until recently, reproducibility of Nd isotope ratios was limited to 15–20 p.p.m. (2σ) using the most precise instruments[13]. This precision barrier has severely hampered application of the ^{146}Sm–^{142}Nd chronometer to terrestrial differentiation because it precludes unambiguous resolution of small ^{142}Nd anomalies. The first claim by Harper and Jacobsen[14] of a 33 p.p.m. excess in a 3.8-Gyr-old Isua metasediment was hence received with scepticism, especially since subsequent studies failed to detect any ^{142}Nd anomaly in the most ancient Archaean terranes[15–17]. More recent

